

Optimal Design of Multilayer Optical Color Filters for Building-Integrated Photovoltaic (BIPV) Applications

Ortiz Lizcano, Juan Camilo; Villa, Simona; Zhou, Yilong; Frantzi, Georgia; Vattis, Kyriakos; Calcabrini, Andres; Yang, Guangtao; Zeman, Miro; Isabella, Olindo

DOI

[10.1002/solr.202300256](https://doi.org/10.1002/solr.202300256)

Publication date

2023

Document Version

Final published version

Published in

Solar RRL

Citation (APA)

Ortiz Lizcano, J. C., Villa, S., Zhou, Y., Frantzi, G., Vattis, K., Calcabrini, A., Yang, G., Zeman, M., & Isabella, O. (2023). Optimal Design of Multilayer Optical Color Filters for Building-Integrated Photovoltaic (BIPV) Applications. *Solar RRL*, 7(19), Article 2300256. <https://doi.org/10.1002/solr.202300256>

Important note

To cite this publication, please use the final published version (if applicable).
Please check the document version above.

Copyright

Other than for strictly personal use, it is not permitted to download, forward or distribute the text or part of it, without the consent of the author(s) and/or copyright holder(s), unless the work is under an open content license such as Creative Commons.

Takedown policy

Please contact us and provide details if you believe this document breaches copyrights.
We will remove access to the work immediately and investigate your claim.

Optimal Design of Multilayer Optical Color Filters for Building-Integrated Photovoltaic (BIPV) Applications

Juan Camilo Ortiz Lizcano,* Simona Villa, Yilong Zhou, Georgia Frantzi, Kyriakos Vattis, Andres Calcabrini, Guangtao Yang, Miro Zeman, and Olindo Isabella

Herein, the application of a comprehensive modeling framework that can help optimize the design of multilayered optical filters for coloring photovoltaic (PV) modules is presented based on crystalline silicon solar cells. To overcome technical issues related to the implementation of color filters (CFs) on PV modules, like glare and color instability, colorimetry metrics, such as the hue, chroma, luminance color space, and the quantitative concept of difference between two colors are extensively deployed. It is showcased in this work that designing colored modules with high hue and chroma stability is possible by using a front-side texturing with edged geometry, like V-shaped grooves and inverted pyramids, while obtaining colors with relatively high luminance values, indicating good brightness. Furthermore, it is argued that adapting the rear surface of the front glass with a random textured layout where the CF is applied can improve color and luminance stability without significant loss of chroma while eliminating glare. Finally, the models can be used to optimize the number of layers for a given CF, reducing unnecessary optical losses. Compared to a standard PV module, performance simulation of optimized, bright-colored PV modules predicts relative energy yield losses ranging from 7% to 25%.

their energy demand.^[2] Efforts toward sustainability in our cities are becoming global and building-integrated photovoltaic (BIPV) systems are considered a key element to achieving near-zero energy buildings.^[3] BIPV solutions can be required to operate under specific conditions, and due to their multifunctional approach, their installation layout is not solely focused on optimized energy yield. One key technical aspect desired on BIPV products for their use on architectural projects is for their aesthetic appearance to be as versatile as possible. Research has shown that, given the option of an aesthetically pleasing solution, customers' interest in installing BIPV systems increases significantly.^[4]

From an aesthetics perspective, color availability ranks high on the potential attractiveness of BIPV solutions.^[5] To achieve this, several techniques are available to change the color appearance

of photovoltaic (PV) modules. For example, implementing ceramic inks has been proven to produce PV modules with an almost unlimited color (and pattern) versatility.^[6,7] Other techniques studied include the use of automotive paints,^[8] colored polymers,^[9] as well as the use of textiles.^[10] The technologies mentioned so far produce colors using absorptive materials. Other approaches focus on light management, like the implementation of resonant nano-scatterers^[11] or the Morpho-color concept, which uses nanostructures that, via interference effects, can produce significant reflectance of light (>60%) on wavelengths that belong to blue, green, and red hues.^[12–14] Finally, other works have focused on the use of multilayer optical filters (OFs) applied either directly on a solar cell or on the front glass layer of a PV module.^[15–17]


Significant efforts have been made to model the impact on aesthetics and performance of the implementation of coloring techniques in PV modules. The approaches are diverse and range from regression analysis to study the relationship between color appearance and electrical output,^[7] machine-learning techniques,^[18] simulations based on model fitting from real measurements,^[19] ray-tracing simulations,^[16,20,21] and fundamental studies that seek to find the theoretical limits in terms of efficiency and power loss based on the spectral characteristics of the solar cells, the color produced, and the light source.^[22] Pelle et al. presents a comprehensive overview of all the

1. Introduction

A paramount goal toward a sustainable future is transforming our urban landscapes from energy consumers to energy producers. The energy required by our cities significantly contributes to CO₂ emissions.^[1] Furthermore, developing countries are experiencing a shift in population distribution, particularly moving from rural areas into urban locations, thus increasing

J. C. Ortiz Lizcano, S. Villa, Y. Zhou, G. Frantzi, K. Vattis, A. Calcabrini, G. Yang, M. Zeman, O. Isabella
Photovoltaics Materials and Devices Group
Delft University of Technology
Mekelweg 4, 2628 CD Delft, Netherlands
E-mail: j.c.ortizlizcano@tudelft.nl

S. Villa
TNO, Energy Transition
High Tech campus 21, 5600 JW Eindhoven, Netherlands

 The ORCID identification number(s) for the author(s) of this article can be found under <https://doi.org/10.1002/solr.202300256>.

© 2023 The Authors. Solar RRL published by Wiley-VCH GmbH. This is an open access article under the terms of the Creative Commons Attribution-NonCommercial-NoDerivs License, which permits use and distribution in any medium, provided the original work is properly cited, the use is non-commercial and no modifications or adaptations are made.

DOI: 10.1002/solr.202300256

forementioned approaches.^[23] In their review work, Pelle et al. argue for the need of a modeling framework that accounts, from the design stage, the potential effect a color technique can have on the PV module's operational temperature and angular behavior. Furthermore, the authors also recommend models that allow flexibility to BIPV manufacturers to study the aesthetic potential of a given technique and provide ways of optimization.

The work presented in this manuscript showcases how a comprehensive modeling framework, developed to study the effect of color filters (CFs) directly applied on solar cells, can be used as a computer-assisted tool to optimize and design colored BIPV module products. This work presents an example of how a color technique can be optimized to find the best balance between color appearance and power production and how some technical challenges can be tackled from the initial design stages to ensure reliable product performance.

The following section discusses an overview of OF design and the modeling framework used in this work. Section 3 follows with a discussion of the color potential of OFs and their technical challenges. Section 4 presents the parameters utilized in this work to optimize the design of CFs, with some proposed design outcomes based on different glass textures. Section 5 studies the impact of these proposed designs on a PV module's electrical performance under different locations. Finally, Section 6 discusses the findings and presents this work's main conclusions.

2. Modeling Framework

This work expands on the research presented in ref. [24], where the entire computational model framework is presented in detail. To explain briefly, the framework is divided into three main pillars: optical, thermal, and electrical model. GenPro4^[25] is the basis of the optical model. The software uses the transfer-matrix and the net-radiation method approaches to calculate the optical behavior of multilayer systems. The outputs used from the optical model are as follows: the values, per wavelength, of reflection ($R(\lambda)$); transmission ($T(\lambda)$), and absorption ($A(\lambda)$), as well as the total optical

current densities (J_{opt}) based on the AM1.5 spectrum for each layer of the optical system. Color perception,^[26] effective irradiance reaching the solar cell (G_{cell}), and solar cell operational temperature (T_{cell}) are estimated based on these outputs. The thermal model has its basis on the finite volume method, with a 2D mesh with nodes distributed throughout the different layers of the PV module. The different thermal properties considered in this study are the same as those presented in ref. [24]. Estimation of the heat generated on the solar cell is performed per wavelength, so that the spectral effects that CFs have on the temperature of the solar cell can be accurately modeled. Other absorptions present on the remaining module's layer are also accounted for. The Gauss elimination technique allows the estimation of T_{cell} for every time instant.

Lastly, both G_{cell} and T_{cell} are used on a two-diode electrical model^[27] to estimate power output at any time instant. The complete validation of these models can be found in Experimental Section at the end of this document.

2.1. CF Considerations

OFs produce color by reflecting light at wavelengths within the visible spectrum. Given that these filters can produce reflection values close to the unity, there is great potential for producing bright colors. This work focuses on very simple OF structures that hold a good potential for large-scale production without incurring significant costs. The simplest way of increasing reflection via OFs is by utilizing two dielectric materials with a mismatch in their refractive indexes. The materials selected here are silicon dioxide (SiO_2), as the material with the lower refractive index (n_L), and silicon nitride (SiN_x), as that with the higher refractive index (n_H). The optical properties of each material and details of their deposition conditions can be found in Appendix of this document. Both materials are considered deposited in pairs (p) on a ($n_L|n_H$) sequence right below the front glass sheet of the PV module. A value of $p = 10$ was selected as a starting point as it was found to ensure a reflection value on flat glass above 0.9 (see **Figure 1a**). Graphically, the OF (henceforth referred as color filter or CF) is represented in this work as shown in **Figure 1b**.

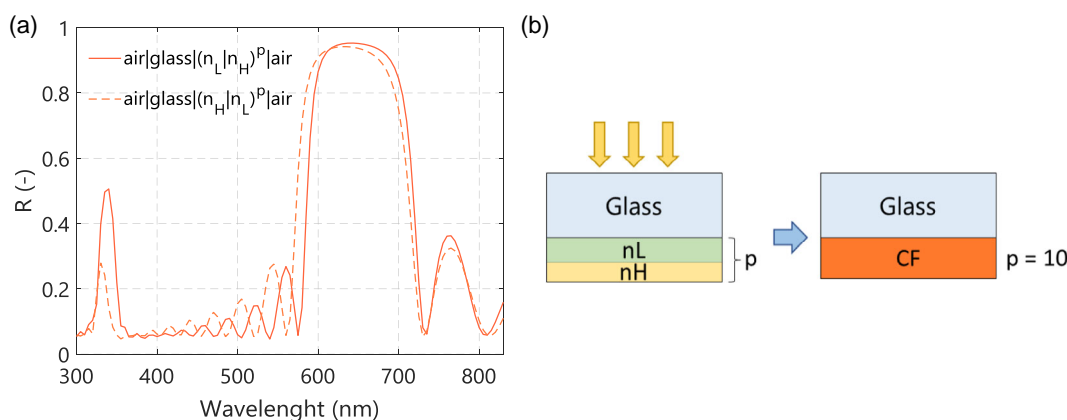


Figure 1. a) In this work, the sequence of the materials of the color filter (CF) follows the $\text{air}|\text{glass}|(n_L|n_H)^p|\text{air}$ layout. When analyzed on flat glass, the sequence produces a slightly narrower reflection band compared to the $(n_H|n_L)^p$ alternative, which helps reduce optical losses. b) For simplicity, the CF is graphically represented as a single-colored layer representing the $(n_L|n_H)^p$ sequence from the top glass downward.

2.2. Effects of the CF on the Performance of a Photovoltaic Module

As demonstrated in ref. [24], the only effect a CF has on the performance of a PV module is a reduced light absorption on the solar cell due to reflection of light. It was also demonstrated that, for the case of an interdigitated back contact (IBC) cell, this effect could be very accurately modeled using scaling factors that are applied on the calculated plane of array irradiance. These scaling factors are denoted as τ_0 and j_{CF} , the former being mathematically defined as

$$\tau_0 = \frac{I_{\text{cell}}}{I_{\text{POA}}} \quad (1)$$

where I_{cell} and I_{POA} are the light intensities calculated on the cell and the front glass of the PV module, respectively. And, the latter is estimated by

$$j_{CF} = \frac{J_{\text{opt color module}}}{J_{\text{opt standard module}}} \quad (2)$$

which is the ratio between the optical current density produced after accounting for the CF, and the optical current density of a standard module without the filter, both estimated at normal incidence of light.

Both scaling factors depend not only on the CF's design, but also on the surface morphology of the different layers of the PV module that interact with light before reaching the solar cell, as will be shown later. A third scaling factor, $j_{\text{opt}(\theta)}$, accounts for the angular optical losses produced by additional reflectance losses due to light reaching the module at an angle of incidence different than 0° (normal incidence). $j_{\text{opt}(\theta)}$ is the ratio between the optical current density of a module illuminated at angle of incidence equal to θ , and the optical current density of the same module under normal incidence. Mathematically, this is expressed as

$$j_{\text{opt}(\theta)} = \frac{J_{\text{opt}(\theta)}}{J_{\text{opt}(0^\circ)}} \quad (3)$$

The reflective behavior of OFs is very sensitive to the angle of incidence at which they are studied. Thus, $j_{\text{opt}(\theta)}$ is characteristic of every module. As stated before, the complete details of the performance model can be found in ref. [24], only τ_0 and $j_{\text{opt}(\theta)}$ are reproduced here given their importance on the design of an optimal CF.

3. CFs: Aesthetic Potential and Technical Challenges

In his seminal work, Angus Macleod^[28] demonstrates that, for an OF with only two different materials, the width of reflectance is dependent on the difference between their refractive indexes. The wavelength at which this reflectance occurs depends on the physical thickness of the layers. Finally, the height of the reflectance depends on the number of pairs deposited.

It was established that for a number of pairs p equal to 10, a CF deposited on a flat glass surface presents reflection values at a given wavelength greater than 0.9. Given that the physical thickness of the OF layers can change the wavelength at which reflectance occurs, the thickness values of both materials, defined as d_L and d_H , were varied from 0 to 200 nm with a resolution of 10 nm. It was found that, for combinations above this range, the color patterns become repetitive, producing similar colors with significantly thicker filters, which was considered not practical.

The reflectance produced by each combination of thickness value was then utilized on a color perception model^[26] to estimate the red, green, and blue (RGB) color coordinates using the mathematical transformation provided within MATLAB's image-processing toolbox for a D65 standard illuminant. These were then used to build color matrices as a graphical representation of the expected color for that given combination. An example of a color matrix for a CF deposited on the backside of a flat glass sheet (as presented on Figure 1b) is presented in Figure 2a. Since the matrix is based on RGB values, a gray

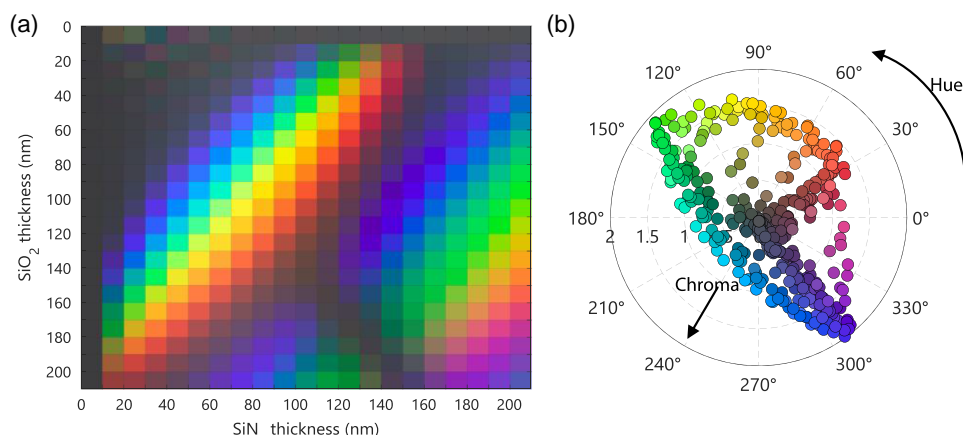


Figure 2. a) Color matrix for different combinations of thickness values for the CF materials selected in this study. The filter is located beneath a flat glass as shown in Figure 1a, with a total number of pairs $p = 10$. The color perception is modeled for the case of an angle of observation (AoO) equal to 0° . b) Representation of the colors depicted on the matrix on the hue, chroma, and luminance (HCL) color space, which is used in this study as an analytical tool for design.

hue represents a transparent perception, not a color. The gray hues indicate that, for that combination of thickness values from the materials, the reflectance peak is within the visible spectrum but is insufficient for color perception, or is located outside the visible spectrum, at the ultraviolet (UV) or Infrared (IR) region. Notice that when the value of one of the materials on the filter is 0 nm, no significant color can be produced, unlike the case of a CF applied directly on a c-Si solar cell, where the variation of the SiN_x layer alone can produce different coloring of the cell. When the value of the thickness of one of the materials is below 30 nm, a higher value of thickness (>100 nm) is needed on the other material to produce good color brightness. In general, for a flat surface, the layout of the selected CF can produce a wide variety of bright colors, ranging from purples all the way to reds.

The utility of the color matrix is to be a guideline to match a particular color to a combination of thicknesses for a given filter layout. It is, however, limited as an analytical tool to optimize its design. A quantitative way of color analysis is the use of color spaces such as the RGB, or particularly, the hue, chroma, luminance (HCL) color space. The HCL color space has been advocated recently over others because it is a perceptual-based color space that does not have saturation bias issues of other alternatives.^[29] Each color is depicted by triplets: the hue value describes the dominant wavelength, and it is represented as a polar coordinate with the range 0°–360°. In this coordinate, 0° depicts red hues, going toward yellows (90°), cyan (180°), blues (270°), and magenta. The chroma coordinate depicts the intensity of the color (also known as colorness) compared to a gray hue under the same conditions of luminance. And, luminance itself defines the brightness of the color. Figure 2b depicts all the colors found on the color matrix of Figure 2a on the HCL color space. Representing the colors that can be produced by a filter in this way allows to see the aesthetic potential of a given layout, both in terms of the hues that can be achieved and their intensity.

Another way in which a color space could be used as an analytical tool for CF design lies in the ability to estimate, quantitatively, the difference between two colors. The color difference standard CIEDE2000 is defined within the HCL color space (polar) by estimating the differences between two colors from their respective CIE L*a*b* color space (Cartesian) coordinates. The mathematical derivation of this standard can be found in the work produced by Sharma et al.,^[30] whose main formula is

$$\Delta E_{00}^* = \sqrt{\left(\frac{\Delta L'}{k_L S_L}\right)^2 + \left(\frac{\Delta C'}{k_C S_C}\right)^2 + \left(\frac{\Delta H'}{k_H S_H}\right)^2} + R_T \frac{\Delta C'}{k_C S_C} \frac{\Delta H'}{k_H S_H} \quad (4)$$

where $\Delta L'$, $\Delta C'$, and $\Delta H'$ are the differences in luminance, chroma, and hue estimated from the two selected colors based on their CIE L*a*b* coordinates. S_L , S_C , and S_H are compensation values for each color coordinate that correct the nonuniformity of the CIE L*a*b* color space. R_T is a rotation term that reduces inaccuracies on the perceived differences in hue and chroma, particularly in the blue region. Finally, k_L , k_C , and k_H are factors that account for the influence of the illumination on color difference perception. A full explanation of their meaning is outside the scope of this work and interested readers can find further information on the work by Sharma et al.^[30] In this work, the estimation of ΔE_{00}^* was done by using MATLAB's image-processing toolbox.

The smaller the value of ΔE_{00}^* the less the discernible difference perceived by the human eye between one color and another. In this work, we explore how the estimation of ΔE_{00}^* can be used to analyze the optimization of a CF, particularly to overcome one important drawback of the technology: its color instability. At different angles of incidence, the optical thicknesses of the different layers within an optic filter change. This change means the wavelength at which constructive interference (high reflectance) occurs differs. Consequently, the perceived color at different angles of observation (AoOs) is not the same as that perceived at normal incidence, as will be explained in the following section.

3.1. Technical Challenges of Colored Filters on Flat Surfaces

Figure 3 shows the decorative potential of utilizing CFs. The result can be a very bright color that can effectively “hide” any object that might be located behind the coated glass. This is particularly attractive for designers that wish to avoid solar cells within a PV module to be visible to any passing observer. However, the photographs also showcase two aspects from the CF that can be considered undesirable.

As an observer moves, the perceived color on the coated glass changes significantly. The deviation from the color observed at normal incidence is very noticeable and, on a large façade arrangement, a continuous change in color can be perceived throughout the glass structure. This phenomenon happens

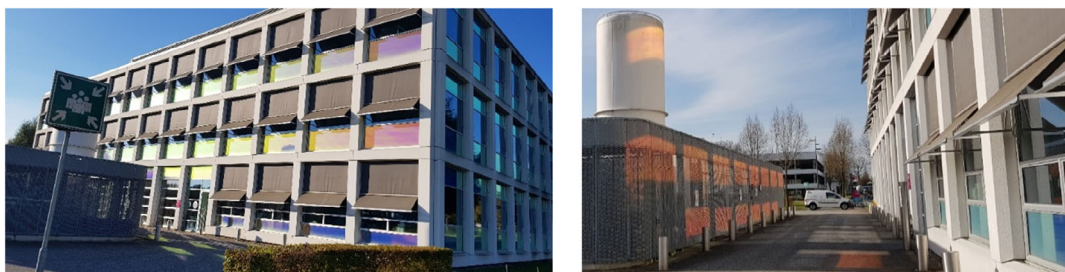


Figure 3. (Left) Colored coated glass on a vertical facade of a building located in the campus of TU Delft. The color shift from window to window is very perceptible, and sometimes undesired. (Right) The coated glass produces substantial glare, which can cause discomfort and must be avoided in critical areas where it could be a potential safety hazard.

because at higher angles of incidence, there is a change in the optical thickness in which light travels through the layers within the filter. This causes a shift in the wavelength at which they produce constructive interference, and, therefore, the observed color changes.^[28]

Another potential issue is glare, which is produced due to the specular nature of the reflectance produced by the CF. Glare is an undesirable aspect on PV modules, particularly those installed on heavily dense urban areas or in proximity to airports, where it can cause safety concerns.^[31]

These drawbacks have been ameliorated by depositing the CF on a textured surface, as explained in the work by Jolissant et al.^[32] Textured surfaces can produce a diffuse reflection of light, eliminating glare substantially. S. Villa^[15] studied how

the deposition of a CF on a random texture surface, produced by Loeff,^[33] could help improve both the issue of glare and color stability. Results showed that when using a CF deposited at the top of a random textured glass as the top layer of a mini-PV module, the glare was reduced completely (see Figure 4 for details).

As mentioned before, depositing the filter on textured surfaces also improves color stability, as demonstrated by A. Wessels et al.^[34]

Utilization of the HCL color space and the ΔE_{00}^* color difference formula can help to analyze how texturization improves color stability. Figure 5a shows the HCL coordinates of the color perceived at different AoOs for the colored mini-PV module shown in Figure 4a. At normal incidence, a bright orange color is perceived, as the AoO changes, a shift on the color perceived

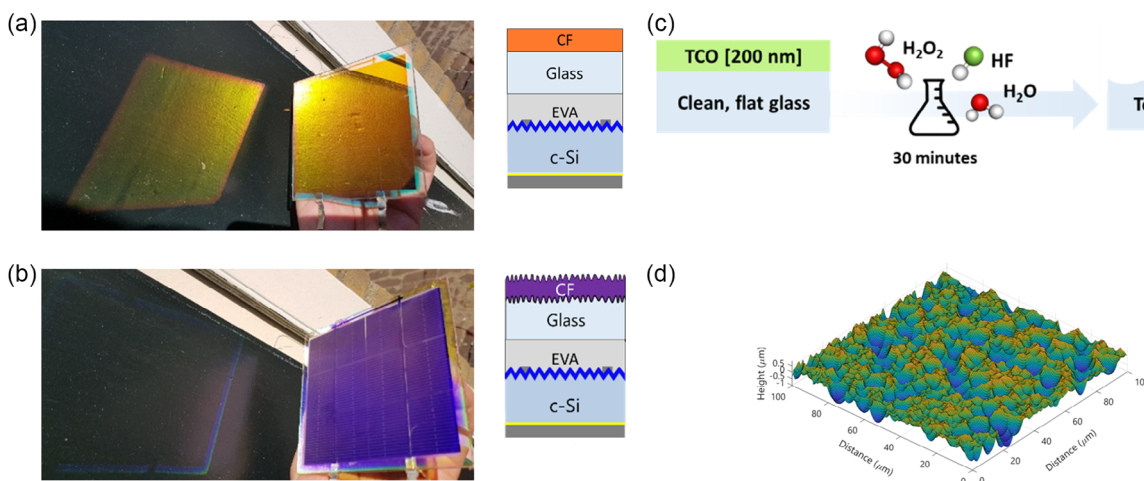


Figure 4. Two different colored mini-PV modules (10 × 10 cm) based on aluminum–back surface field (Al–BSF) laser-cut solar cells. a) An orange CF deposited at the top of flat glass ($p = 10$, $\text{SiO}_2 = 90$ nm, $\text{SiN}_x = 100$ nm), which produces significant glare. b) The glare is completely reduced by deposition of the CF on a randomly textured glass ($p = 10$, $\text{SiO}_2 = 68$ nm, $\text{SiN}_x = 164$ nm). More information about these results can be found in the work of S. Villa.^[15] c) Wet–chemical etching procedure of glass mediated by transparent conductive oxide.^[44] d) Atomic force microscope image of a typical etched glass used for improving color stability (statistical data of the randomly textured surface can be found in the work by Loeff^[33]).

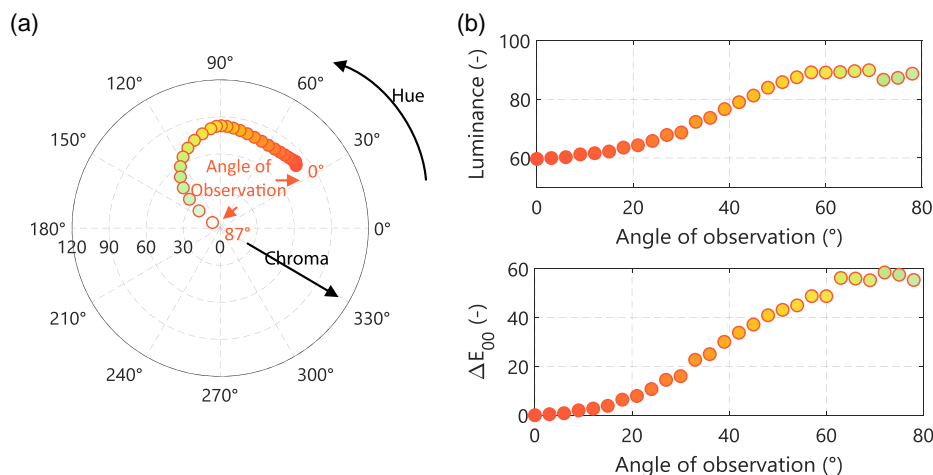


Figure 5. a) HCL color space representation of the change in color perception as a function of AoO for a colored mini-PV module based on the structure shown in Figure 4a. On flat surfaces, color stability is limited. b) Change on the value of luminance L (top) and ΔE_{00}^* for increasing AoOs.

occurs, driven by the changes on the optical paths, as explained before. Notice that the main change is in the hue coordinate, rather than the chroma coordinate, which indicates that selective reflection is still high. However, as the AoO increases toward large angles ($>60^\circ$), the hue stabilizes and the chroma becomes smaller. This means that the selective reflection is lost, and the color disappears. Figure 5b shows how the factor ΔE_{00}^* changes at different angles of observation. For this case, color stability is only limited to low AoOs ($<20^\circ$).

When the CF is deposited on the randomly textured glass, the color stability partially improves compared to the case of the filter deposited on flat glass. Figure 6a shows how the hue coordinate remains remarkably stable, with only a few degrees of variance between normal incidence and an AoO of 87° . Significant changes in the color occur on the chroma coordinate, however, meaning a loss in color brightness due to increased front surface reflection. This is evident on the estimation of the ΔE_{00}^* value, as shown in Figure 6b. Notice that, to highlight color differences

graphically, in both Figure 5 and 6, the markers are filled with the perceived colors at any given angle of observation. In contrast, the outline lines are colored with the perceived color at normal incidence.

Random textures are therefore a promising surface modifying technique for CF implementation when glare effects need to be removed, moreover, as shown in Figure 7, the range of hues and chromas is quite variable and appealing. Compared to a filter deposited on a flat glass, there are losses on purple and blue hues, but not by a considerable amount. However, positioning the filter at the top of the front glass of a PV module not only can lead to problems with the integrity of the filter itself, which might reduce its usefulness, but also does not guarantee color stability.

Figure 5b and 6b also present the changes in the luminance values concerning the AoO for a CF deposited on a flat glass surface and a randomly textured glass surface, respectively. At normal incidence, the CF deposited on a flat glass presents a higher luminance value than the deposition on a random

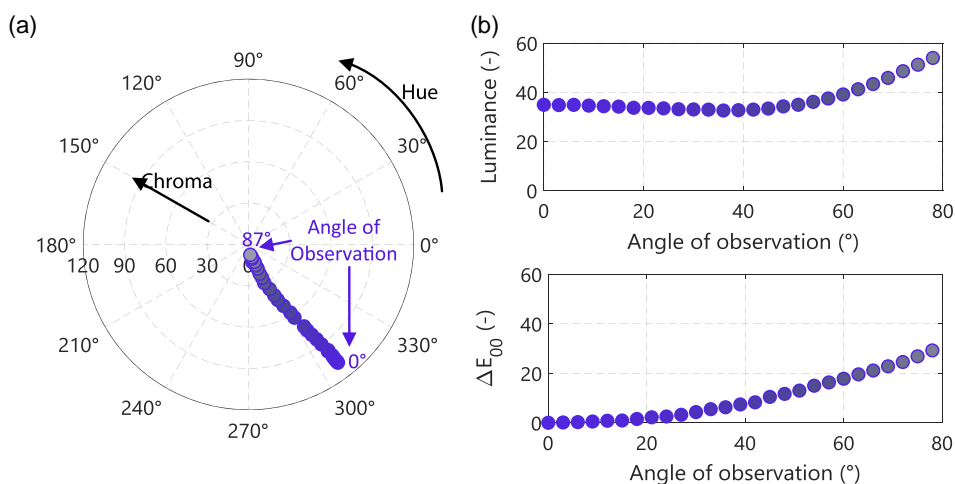


Figure 6. a) HCL color space representation of the change in perceived color for different AoOs for a mini-PV module as shown in Figure 4b. The texture surface provides impressive color stability and maintains high values of chroma. b) Calculated luminance L (top) and ΔE_{00}^* value for the same structure.

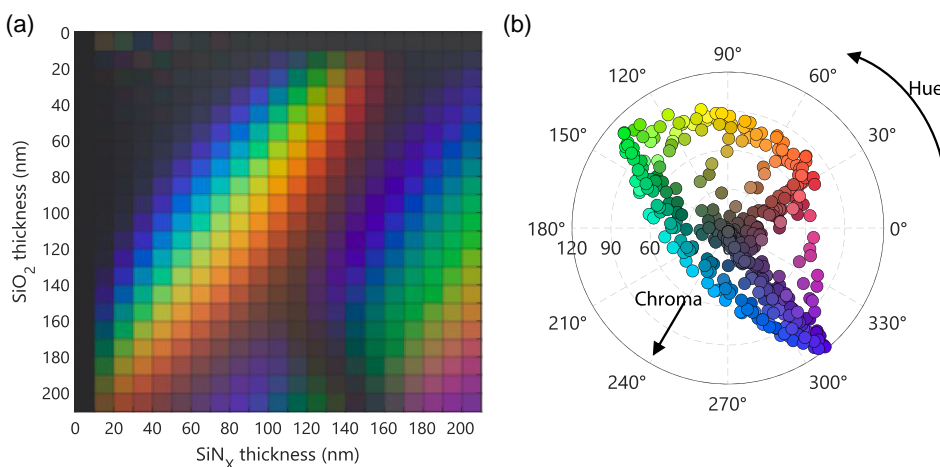


Figure 7. a) Matrix of the perceived colors produced by different combinations of thicknesses of $\text{SiO}_2/\text{SiN}_x$ ($p = 10$) of a CF deposited on a randomly textured glass similar to that reported in Figure 4d. b) HCL representation of all the colors reproduced on the color matrix.

textured glass, which translates into a brighter perception of the color from the flat sample. As the AoO increases, the luminance of both colors follows the same trend. For the case of the flat sample, at high AoOs, the reflectance from the front glass increases in a broader range of wavelengths, decreasing color strength and making its perception closer to a white color. Thus, even when the chroma coordinate decreases rapidly, the luminance increases, almost reaching its limit. The observed behavior on the textured sample is similar. However, in this case, the reflectance peak shifts from the blue region to the UV outside of the visible spectrum, producing a color loss. The value of luminance at high angles of incidence is significantly lower than the case of the flat sample, meaning the perceived color is closer to a gray color than white.

4. Optimal Design of Colored Filters Based on Colorimetry Parameters

Placing the CF beneath a thick glass layer protects it against environmental hazards but could potentially change its overall behavior. To study this effect, an optical system, as described in **Table 1**, was modeled. The selected c-Si cell structure was based on the Maxeon III IBC solar cell from SunPower.^[35] The cell was in-house measured, and the optical model was fitted to its behavior (see Experimental Section).

To study the effect that the texturing of the front glass has on color stability, HCL coordinates were calculated for the case of a CF with $\text{SiO}_2 = 90 \text{ nm}$ and $\text{SiN}_x = 100 \text{ nm}$ for a value of $p = 10$. The AoO varied from 0° to 87° with a resolution of 3° .

Different types of front-side texturing were analyzed and compared to the case of flat glass. Three types of texturing were analyzed: an inverted pyramidal structure with depths up to $250 \mu\text{m}$ and a steepness of 45° ; a rounded groove like Saint-Gobain's Albarino P^[36] with depths equal to $250 \mu\text{m}$; and a V-shaped texture with an angle of 45° and a depth of $500 \mu\text{m}$ that mimics Saint-Gobain's Albarino G series.^[36] These front-side layouts were paired with one of two options for the backside, where the CF is placed: a flat surface, and the random textured surface utilized by S. Villa.^[15] These two layouts were selected given that the optical behavior of the CF could be experimentally validated. The selected structures are shown in **Table 2**, and a graphical description of these geometries is presented in Supporting Information.

Analysis of other structures in which the CF can be deposited is outside of the scope of this study, as some of them require

Table 1. Selected optical system for color filter design (* = estimated value based on fitting).

| Layer | Thickness | Optical properties |
|--------------|--------------------------------|----------------------------------|
| Glass | 3.2 mm | Taken from ref. [45] |
| Color Filter | Varied [0–0.2] μm . | See Appendix |
| EVA | $p = 10$ | |
| EVA | 0.5 mm | Taken from ref. [46] |
| c-Si | 0.18* mm | Fitted according to measurements |

Table 2. Structures simulated to study the effect on color stability of different texturization layouts.

| Glass texture layout | | | |
|----------------------|------------------|-----------------|--------|
| Structure no. | Front | Rear | Symbol |
| 1 | Flat | Flat | □ |
| 2 | Rounded grooves | Flat | ○ |
| 3 | Rounded grooves | Random textures | ○ |
| 4 | V-shaped grooves | Flat | △ |
| 5 | V-shaped grooves | Random textures | △ |
| 6 | Inv. pyramids | Flat | ☆ |
| 7 | Inv. pyramids | Random textures | ☆ |

specific and complex additional optical modeling to accurately predict the growth of the CF layers and the correct optical paths resulting from their manufacturing. One example of the additional modeling required can be found in the work by Wessels et al.^[34]

Figure 8 summarizes the effect that texturing has on the perceived color for the same combination of thicknesses ($\text{SiO}_2 = 80 \text{ nm}$ and $\text{SiN}_x = 80 \text{ nm}$ and $p = 10$). Structures 2 and 3, which feature rounded grooves at the front side of the glass and flat (Figure 8b) or random texture (see Supporting Information) at the rear side of the glass, respectively, only slightly ameliorate color stability at different AoOs. Color stability only improves when the geometry of the front glass consists of edged geometry. V-shaped grooves significantly improve the stability of the color at the expense of loss in chroma. At different observation angles, the green color produced with a V-grooved glass has only marginal changes on the chroma coordinate, and the hue coordinate can be contained within the green region (Figure 8c). Compared to a V-shaped geometry, an inverted pyramidal texture improves color stability over a wider range of observation angles, as seen in Figure 8d. The hue coordinate remains stable with a slight gain in chroma. Only at values of AoO, above 60° does the hue coordinate change. Deposition of the CF on a randomly textured surface provides better color stability, as shown in Figure 8e. Moreover, the random texture does not reduce luminance but stabilizes it (see Figure 8f).

In summary, texturing the front side of the module's glass with edge geometries provides good color stability, even when the CF is on a flat backside surface. Inverted pyramids are the best front surface configuration for luminance stability. Deposition of the CF on a random texture surface presents the best luminance stability and slightly improves color stability. **Figure 9** showcases the aesthetic potential of all the structures analyzed in this work. CFs deposited on flat surfaces have a wider range of chroma, particularly in the case of glass with front V-shape grooves. This structure can obtain bright yellows but not reds. Green and purple colors can achieve chroma values close to their respective limits. A front texture based on inverted pyramids with a steepness of 45° presents a more limited chroma range. Bright yellow colors are not possible for this texturing configuration and thickness combinations. However, highly saturated purples, blues, and greens are still possible.

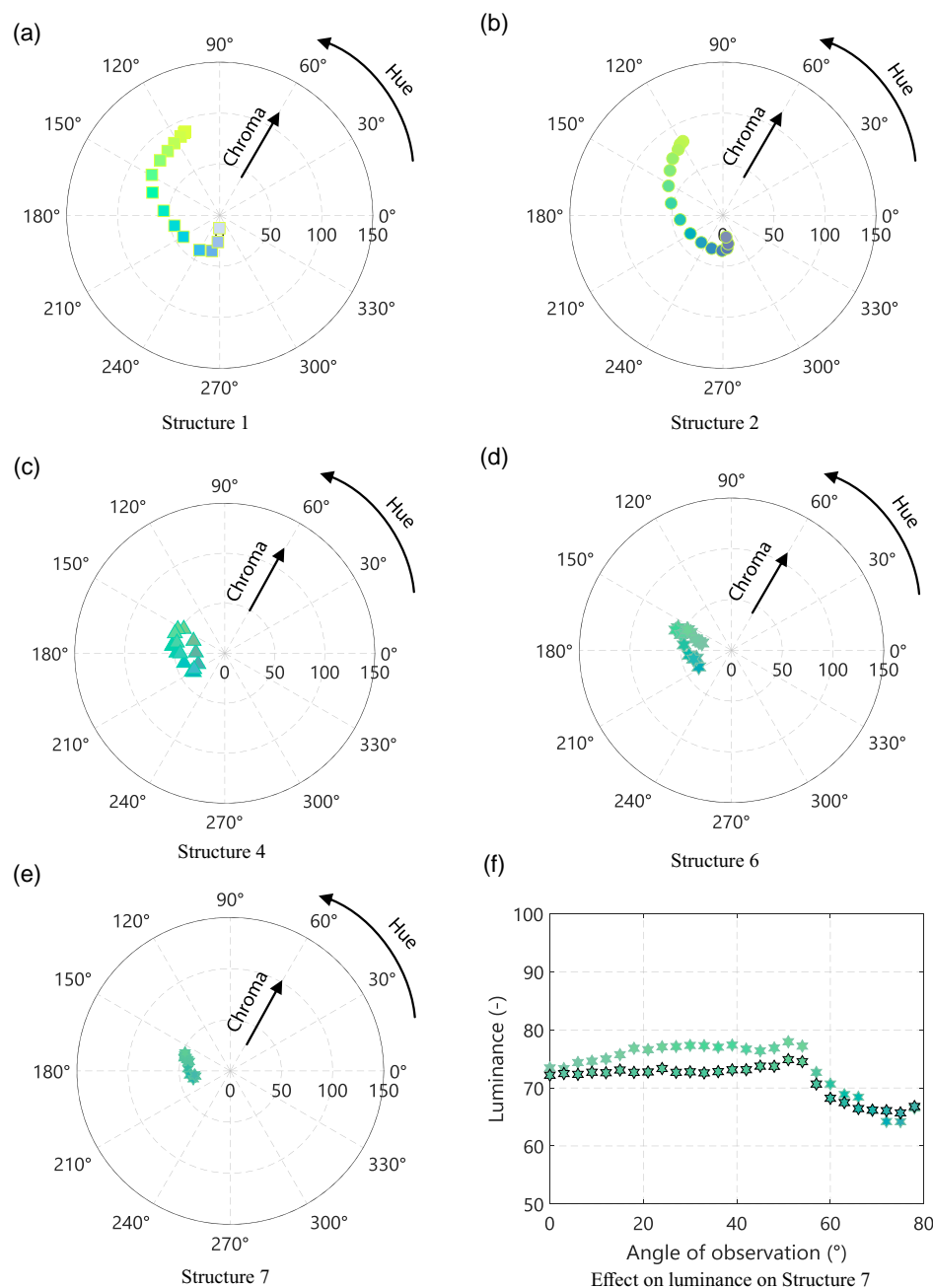


Figure 8. a–e) Color stability analysis for five of the different structures presented in Table 2. f) A CF with $p = 10$ deposited on the flat back surface of a front textured glass (inverted pyramids) presents values of luminance that slightly increases at different observation angles (hexagrams without black edges). Deposition of the CF on a random textured surface improves luminance stability (hexagrams with black edges).

The aforementioned does not mean brighter colors, including yellow, cannot be obtained with an inverted pyramid texturing surface. Reducing the pyramid steepness angle and depth can improve HCL, as the surface will behave closer to the case of flat glass. However, doing this also means that color stability will decrease. Further investigation of the potential of this geometry is underway.

Regarding luminance, the textured layouts studied cannot produce the wide range of bright colors obtained by the double flat glass. V-shaped grooves and inverted pyramid layouts can produce colors with high luminance but are usually limited to green, blue, and brown hues (see Supporting Information). Another example of texturing that can produce vibrant colors is the Morpho Color concept.^[13]

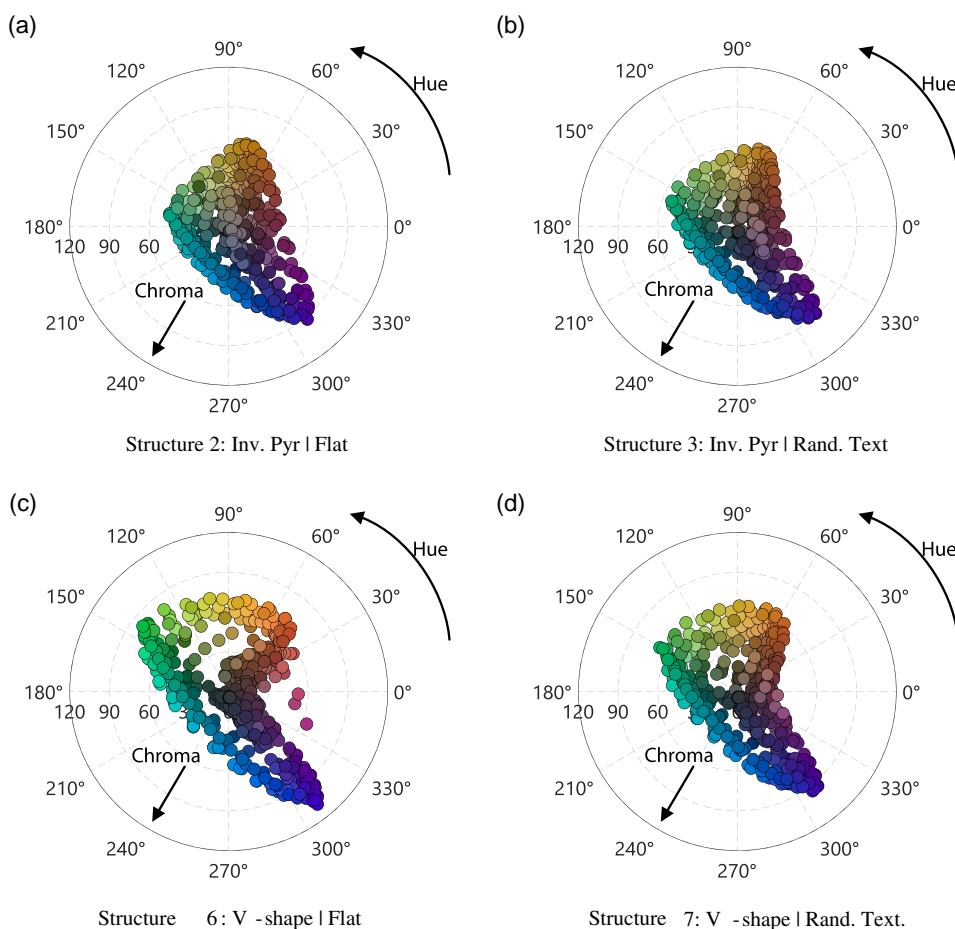





Figure 9. Hue and chroma variations for different PV module glass texturing (top side | back side) layouts: a) Inverted Pyramids | Flat (Structure 2). b) Inverted Pyramids | Random textures (Structure 3). c) V-shape | Flat (Structure 6). d) V-shape | Random textures (Structure 7). More information of these layouts is presented on Table 2 and in the Supporting Information. For all cases, the colors are those obtained from a CF with a number of pairs $p = 10$.

4.1. Optimized Number of Layers for Color Perception

Stabilizing color is, from a PV module performance point of view, stabilizing the value of $j_{opt(\theta)}$. A stable color means that the peak of reflectance remains close to its wavelength value at normal incidence, thus, the value of $j_{opt(\theta)}$ at various AoOs becomes close to unity. Also, designs that involved thin CFs with small layer counts are preferred due to their ease in manufacturing. The color difference formula can be deployed to find if the initial number of pairs (p) considered for a given design can be reduced without any loss in color perception. Structure 7 was selected since it showed the best combination of chroma, hue, and luminance stability among all the samples studied. The three colors selected, which belong to different hue coordinates, are presented on Table 3.

Given that the number of pairs had an initial value of 10, the color produced by this CF design was considered as the reference. The value of p was increased up to 13 and reduced until reaching a value of 4. For each iteration, the value of ΔE_{00}^* is

Table 3. Selected color filters for the optimization of number of pairs without perceivable color change.

| Color 1 | Color 2 | Color 3 |
|---|---|---|
|  |  |  |
| $p = 10$ | $p = 10$ | $p = 10$ |
| SiO ₂ = 80 nm | SiO ₂ = 100 nm | SiO ₂ = 90 nm |
| SiN _x = 80 nm | SiN _x = 140 nm | SiN _x = 100 nm |

calculated with respect to the color produced with $p = 10$. Figure 10a shows how the value of ΔE_{00}^* changes for different values of p for Color 1. For the sake of clarity, the squares on the insert in the graph depict the color perceived according to the number of pairs. This was done to demonstrate that for a value of $p = 6$, a change in the color can be perceived and becomes

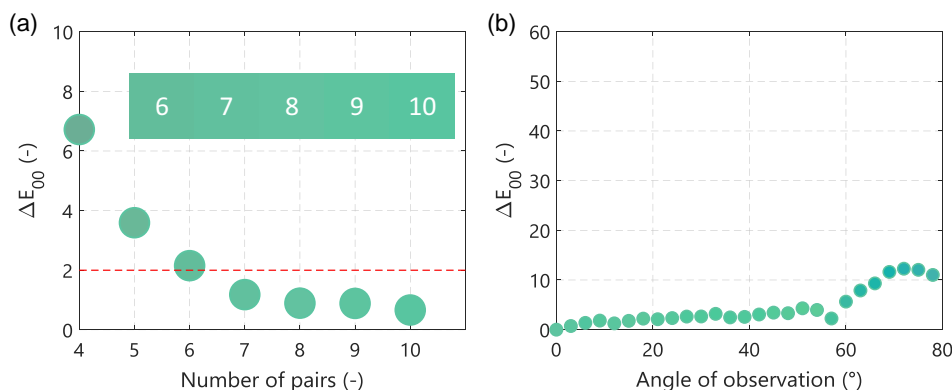


Figure 10. a) Changes on the value of ΔE_{00}^* by modifying the number of pairs for Color 1. b) Value of ΔE_{00}^* for different AoO to study the color stability of the final design based on $p = 7$. Notice that the selected limit value for ΔE_{00}^* to optimize the value of p only applies for the optimization of color perception at normal incidence. ΔE_{00}^* different AoO is only used as an analytic metric to color stability.

evident at lower values of p . For the optimization of the number of pairs, the limit $\Delta E_{00}^* = 2$ was selected as the maximum allowed ΔE_{00}^* value. Results indicate that, to produce Color 1, the filter can be reduced from 10 to 7 pairs with just a slight loss on the color perceived.

$\Delta E_{00}^* = 2$ is only used as a limiting value for the case of normal incidence of light to optimize the value of p . When analyzing the color stability at different AoOs, ΔE_{00}^* serves only as an analytical metric, with no selected limiting value.

This same process of optimization allowed to find the value of p for Color 2, Color 3, and all combinations of thicknesses presented in this work. For the selected limit value of $\Delta E_{00}^* = 2$, the optimum value of p for the different colors is showcased in Figure 11.

Divergence on the value of p can be explained by the fact that human perception of color differences have been found by some studies to be lower for some hues (particularly yellow) compared to others (like blue).^[37]

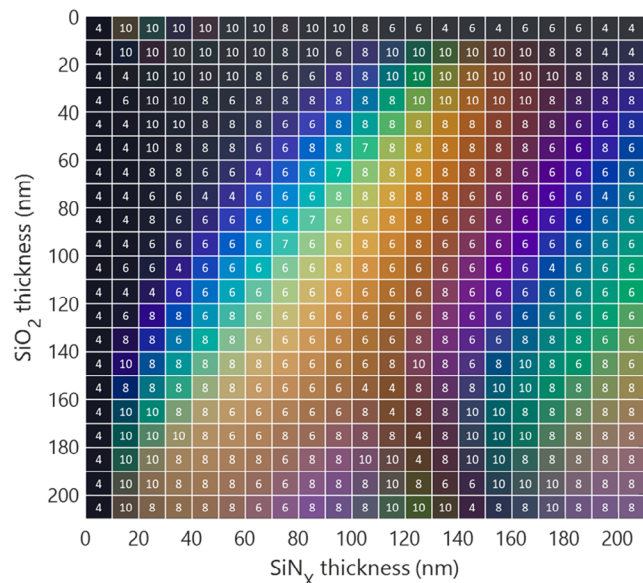


Figure 11. Optimized number of pairs for filter without significant loss on color perception.

5. Effect of the CFs on the Performance of a c-Si PV Module

Implementing a CF on a PV module, as described in ref. [24] has two main effects that affect the overall performance of the solar cell. The additional optical loss reduces the generated current on the cell, which lowers the electrical efficiency of the colored module. However, this same reflection loss reduces the operational temperature of the cell, which is beneficial for performance. Estimating both G_{cell} and T_{cell} is paramount in accurately modeling the effect that a CF has on the performance of a PV module. To this end, experiments were carried out using both mini modules presented in Figure 4 to assess the accuracy of the models presented in ref. [24]. The measured reflectance from both mini modules at different angles of incidence was compared to those obtained via the optical model. The results indicate good agreement for the case of the flat CF (RMSE = 2.36%) and reasonable agreement for the CF deposited on the random textured glass (RMSE = 5.65%). Due to technical constraints, creating a fully functional textured sample was impossible. For this reason, the thermal and electrical models were validated by measuring the orange mini module (flat sample). Comparison between the simulated and measured temperatures for 12 days produced an RMSE value of 1.15 °C. Lastly, simulated current–voltage (I – V) curves had an RMSE below 1% for power generated once the value of the scaling factor j_{CF} was applied to the two-diode model of the standard module. Detailed information from the experiments is presented at the end of this manuscript.

Figure 12 showcases the difference in absorbed and extracted irradiance power on a c-Si solar cell for a) the standard module compared to b) a color module under nominal operational cell temperature (NOCT) conditions. The latter case shows a reduction of the thermalization losses, which reduces operating temperature but also the extracted power.

The optimization conducted in the previous section focused on reducing the number of pairs within the filter without significant loss on color perception. Lowering the number of pairs translates, as demonstrated by Macleod,^[28] on a reduced reflection peak. This means a lower value of the factor j_{CF} and an increased optical current on the optimized design, but also might

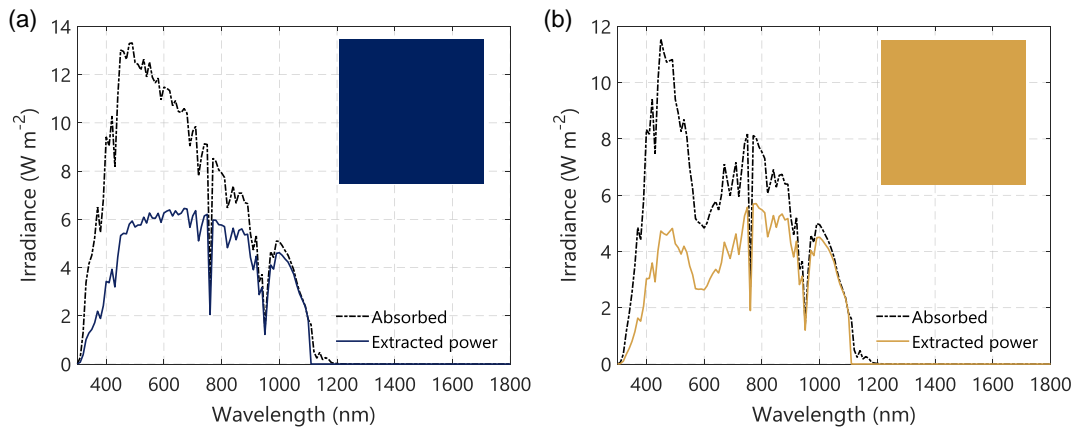


Figure 12. Absorbed and extracted power of a) standard module under nominal operational cell temperature (NOCT) conditions and b) module with the filter Color 3, under the same conditions. Reflection of light to create the color produces a dual effect on the overall performance of a PV module. Reduction of extracted power, which reduces electrical performance, and a reduction of the total absorbed irradiance, which reduces a cell's operational temperature. Overall, the optical loss created by the color dominates, and it is never compensated by a reduced operational temperature.

translate on an increased operational temperature. The effect of this optimization is presented on **Table 4**, with the optical currents estimated under standard test conditions (STCs).

Color 1 with a value of $p = 10$ presents a relative loss on the optical current density of 16.65% when compared to a standard module. Optimizing the number of pairs reduces this loss to 15.69% without incurring noticeable losses in color perception. For the case of Color 2, the optimization causes the relative loss in optical current density to go from 24.65% to 23.56%. For Color 3, the optimization produces a relative loss change from 21.47% for $p = 10$ –20.28% for $p = 6$. With respect to operational temperature, **Table 4** shows that producing Color 1 reduces the operational temperature by almost 7.31 °C, whereas Color 2 and Color 3 present reductions of 7.22 and 7.81 °C, respectively. Optimizing the number of pairs increases the temperature under NOCT conditions of Color 1 by 3.06 °C. Optimization of Color 2 and Color 3 produces increased temperatures under NOCT conditions of 3.12 and 3.27 °C.

Overall, optimizing the number of layers contributes to a better electrical performance of the colored modules. The two-diode

model was used for estimating the J – V curves of a single solar cell operating under the different module layouts studied. Equation (2) was deployed to scale down the effective irradiance reaching the solar cell. Results are presented in **Figure 13** for the case of Color 1 and on **Table 5** for all the colors under STC and NOCT conditions.

Under NOCT conditions, a cell on a module with a CF, thanks to its reduced operational temperature, reduces the gap difference in power produced compared to a similar cell under a standard module layout, as shown in **Table 5**.

In general, the gains produced by the reduction of operating temperature do not compensate for the loss produced by the additional reflection loss. For all the thickness combinations discussed in this work, the CF always produces less electrical energy than a standard module.

Calculations of the annual yield were performed to assess the overall effect that implementing a CF on the front glass has on the performance of a solar cell. The selected locations were, as the case presented in ref. [24], Delft in Netherlands, and Alice Springs in Australia. The higher frequency of clear skies in Australia proved to be slightly more beneficial due to lower operating temperatures from the color modules. At both locations, two different installation layouts were analyzed, a module tilt of 35°, for a rooftop PV system, and a façade layout, with a tilt equal to 90°. On both cases, the optimum azimuth was considered.

The annual yield of a single IBC solar cell in Delft under a standard module layout was estimated at 3.65 kWh year⁻¹ for the case of a rooftop PV system, and 2.38 kWh year⁻¹ for the case of a PV façade. At Alice Springs, these values were found to be 6.81 and 3.22 kWh year⁻¹, respectively. The color matrix for the optimized filter designs is presented below for both locations, with the relative loss indicated, in percentage, when compared to the values mentioned earlier.

Figure 14 showcases that there is a possibility of producing colored modules with blue, green, purple, maroon, and gold with relative losses below 14%. Some combinations of thicknesses can produce similar hues with significantly higher relative losses

Table 4. Effect of the layer optimization on the optical current density (J_{opt} @STC), the irradiance scaling factor j_{CF} (@STC), and the operational cell temperature (T_{cell} @NOCT) for the three selected colors.

| | Standard | Color 1 | Color 2 | Color 3 |
|--|----------|---------|---------|---------|
| J_{opt} [mA cm ⁻²] | 42.26 | 35.22 | 31.84 | 33.19 |
| j_{CF} [–] | – | 0.83 | 0.75 | 0.78 |
| J_{opt} [mA cm ⁻²] p optimized | – | 35.63 | 32.30 | 33.69 |
| j_{CFopt} [–] | – | 0.84 | 0.76 | 0.79 |
| $T_{cellNOCT}$ [°C] | 47.32 | 40.01 | 40.10 | 39.51 |
| $T_{cellNOCT}$ [°C] p optimized | – | 43.07 | 43.22 | 42.78 |

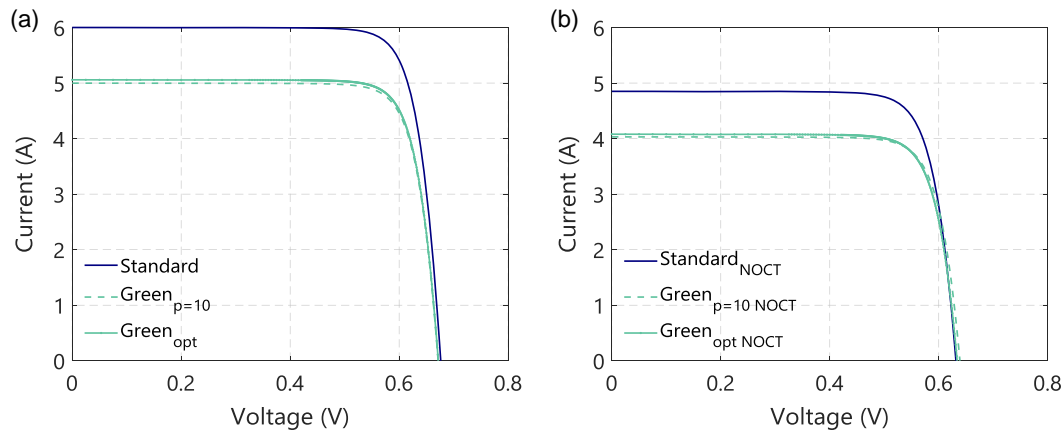




Figure 13. a) Current density–voltage (J – V) curves of a single solar cell under a standard module layout, or a module with a Color 1 filter with $p = 10$ layout, or a module with an optimized Color 1 filter in standard test conditions (STC). b) J – V curves of a single solar cell under standard module layout or optimized Color 1 module layout in NOCT conditions.

Table 5. Power produced (W) by a single solar cell under the module layouts depicted by the colors. And the relative loss for the optimized color cases when compared to a standard layout.

| |  |  |  |  |
|--------------------------|---|---|---|---|
| P_{STC} [W] | 3.31 | 2.76 | 2.47 | 2.60 |
| P_{STC} optimized [W] | – | 2.79 | 2.53 | 2.64 |
| Relative loss [%] | – | 15.69 | 23.56 | 20.28 |
| P_{NOCT} [W] | 2.45 | 2.09 | 1.87 | 1.97 |
| P_{NOCT} optimized [W] | – | 2.09 | 1.89 | 1.98 |
| Relative loss [%] | – | 14.69 | 22.85 | 19.18 |

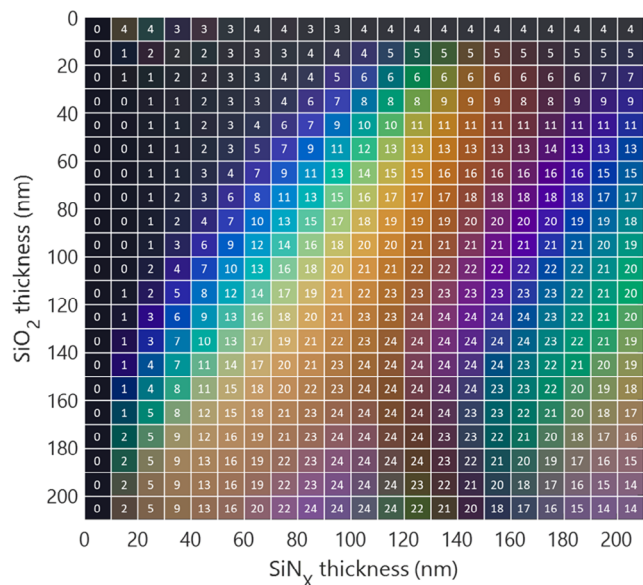


Figure 14. Relative DC energy yield loss (in percentage) for different colored modules when compared to a standard module ($EY = 3.65 \text{ kWh year}^{-1}$) for Delft (rooftop PV module tilt = 35° oriented south).

(>20%). Additionally, the relative losses of a few colors are lower in a location with higher frequency of clear skies, like Alice Springs, as presented on **Figure 15**. The relative DC yield losses remain remarkably stable for the case of the PV façade, with comparative changes below 2% compared to the case of the rooftop PV, as presented in Supporting Information. As mentioned earlier, one of the main benefits of color stabilization, from an energy yield perspective, is that the value of $j_{opt(\theta)}$ (Equation (3)) remains very stable for a wide range of angles of incidence. The main loss comes from the reflectance provided to create the color, and its stability translates into similar relative performance under different installation layouts.

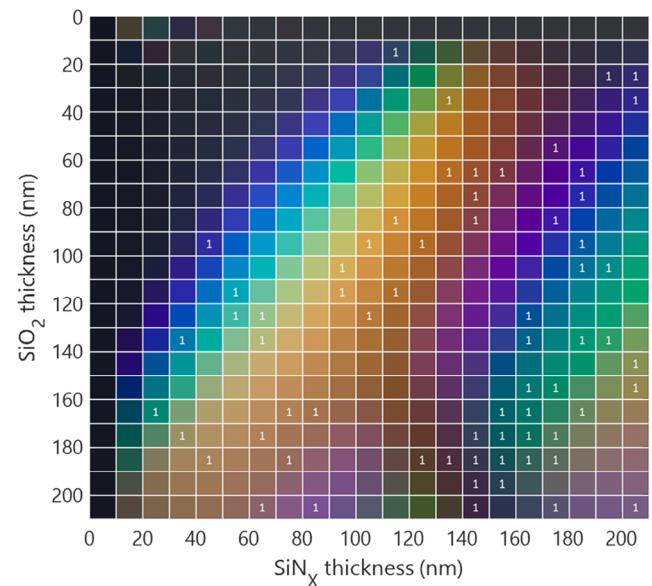


Figure 15. Difference on the relative DC energy yield losses at Alice Springs for the different color modules compared to the case of Delft (Figure 14). Positive numbers indicate a reduction in the relative DC energy yield losses when compared to a standard module. For most colors, the relative loss remains equal on both locations. On the exceptions, the improvement on performance is never above 2%.

6. Conclusions

The proposed modeling framework presented in our previous publication, in combination with colorimetry concepts, is used in this work as computational aiding tools for the design of colored modules for BIPVs based on c-Si technologies. The models can help find the optimal texturing layout for color stability, assess the HCL losses of a given CF layout, and estimate the simplest filter design for a desired color.

Experimental activities were conducted to validate the accuracy of the spectrally resolved models, producing good agreement on all three main pillars: optical, thermal, and electrical. The calculated RMSE error for the case of a CF deposited on flat glass was 2.36%. For the case of a CF deposited on a random textured glass, the value of the RMSE was 5.65%. The angular behavior of the textured sample was measured and compared to simulation results. The optical model presents high RMSE values at AoOs above 70°. A possible explanation for this lies in the assumption of the optical model that the growth of the layers of the filter during deposition is homogeneous in all directions of the texture. Improvements in this matter will continue in future work.

The thermal model showed RMSE values of 1.15 °C for both a standard and a colored module (flat glass) for a time resolution of 10 s over for a period of 11 days.

The accuracy of the electrical model is highly dependent on the accuracy of the optical model, with low error on the latter, the former can produce highly accurate results.

Utilization of the color difference factor ΔE_{00}^* and the HCL color space is key to produce high performing designs both in terms of electrical output as well as aesthetic approaches. ΔE_{00}^* can be used on the assessment of the color stability of a given CF layout. Seven structures were studied using ΔE_{00}^* , from the combination of three front texture geometries for the front side of the PV glass and two layout options for the backside: random texture and flat. Results showed that hard-edged geometries, like V-shaped grooves or inverted pyramids substantially improve color stability. HCL color space analysis indicates that texturing the backside of the module, where the CF is to be deposited, improves luminance stability with the bonus of eliminating any potential glare. Overall, simulation results indicate that a combination of an inverted pyramidal texturing on the front glass and the CF deposited on a random textured surface (structure 7) showed greater color stability when compared to other alternatives.

Analysis of ΔE_{00}^* also helps reduce unnecessary optical losses by reducing the number of layers of a given CF, without significant sacrifice in color perception. Optical current densities resulting from the three selected CFs deposited on a random textured glass were increased up to 1.2% by using this approach.

When analyzing other effects on performance, the additional reflection produced by the CF has a dual effect on a solar cell. The additional optical loss causes a reduction in the current generation. However, this same loss produces a lower operational temperature than the standard case. Electrical calculations performed at STC and NOCT conditions lead to the conclusion that the optical loss is not fully compensated by the thermal gain; however, at higher operating temperatures, the relative electrical loss on a colored module is lower than the case of STC.

Finally, calculations of the expected yearly DC energy yield for two installation layouts (rooftop PV and PV façade) showed that the overall losses produced by the CFs are almost independent of the location they operate. Locations with a high frequency of clear skies present slightly lower relative energy yield losses than locations with more frequent overcast days. These findings indicate that the benefits from lower operational temperatures do not translate into significant gains in electrical performance. Furthermore, differences on the relative DC yield losses between the two installation layouts studied were also small due to the efforts to stabilize the color. This stabilization translates into very small additional angular losses.

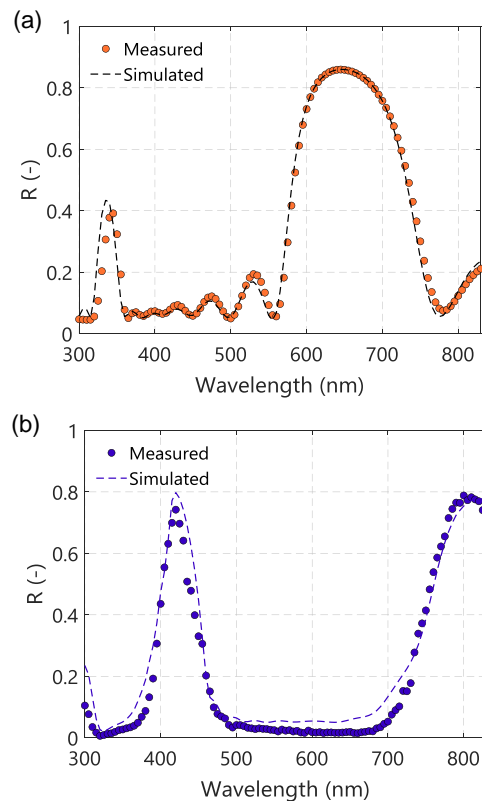


Figure 16. Measured and simulated reflectance of a CF deposited on the front glass of a PV mini module: a) an interdigitated back contact (IBC) solar cell encapsulated with a flat glass and the CF deposited below the glass (orange); b) a set of Al-BSF laser-cut solar cells encapsulated with a random textured front glass with the CF deposited on top (purple), see Figure 4b.

Table 6. Values of MAE, MBE, and RMSE for the assessment of the accuracy of the optical model for both colored mini modules.

| | Orange | Purple |
|------|--------|--------|
| MAE | 1.24% | 4.53% |
| MBE | -0.42% | -3.54% |
| RMSE | 2.36% | 5.65% |

Generally, a sizeable number of hues can be produced with relative energy yield losses below 20%, with some CFs showing losses as low as 7%.

7. Experimental Section

The electrical models presented in ref. [24] were validated on first instance via comparisons between the two-diode model approximation with simulations carried out on Sentaurus TCAD. The thermal model was validated by comparing the predicted temperature of a standard PV module with measurements carried out on non-colored solar modules. For this work, both the thermal and the electrical models were validated by making direct comparisons with colored mini modules.

The mini modules were manufactured by encapsulating two SunPower Maxeon Gen III solar cell. One of the solar cells was encapsulated on a standard glass | EVA | cell | EVA | Tedlar layout, while the other one had the glass | CF | EVA | cell | EVA | Tedlar. The selected CF was made of six pairs

of SiO₂ | SiN_x layers, with thicknesses of 90 and 100 nm, respectively. For the case of the CF deposited on a random textured glass, the demonstrator manufactured by S. Villa^[15] was used. The results from the measured and simulated reflectance for each CF are shown later **Figure 16**.

For both cases, the metrics used to assess the accuracy of the prediction were the mean bias error (MBE), the mean absolute error (MAE), and



Figure 18. Temperature measurements of a colored mini module (orange, left), a mini module with an experimental filter (middle, outside of the scope of this work) and a standard mini module (right).

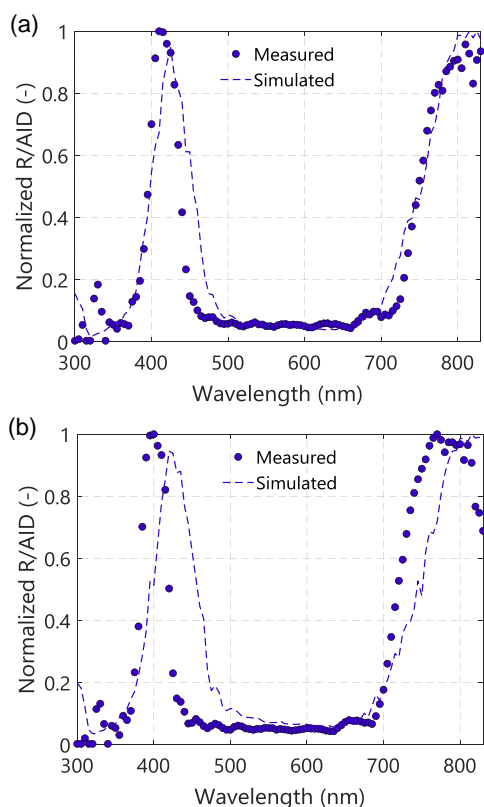


Figure 17. Simulated normalized reflectance compared con the measured angular intensity distribution (AID) obtained with the spectrophotometer with an ARTA device for two AoOs of a) 50° and b) 70°.

Table 7. Values of MAE, MBE, and RMSE to assess the accuracy of the predicted angular behavior of a purple CF deposited on a randomly textured surface.

| | 50° | 70° |
|------|--------|--------|
| MAE | 6.72% | 14.84% |
| MBE | -2.65% | -1.90% |
| RMSE | 11.30% | 23.80% |

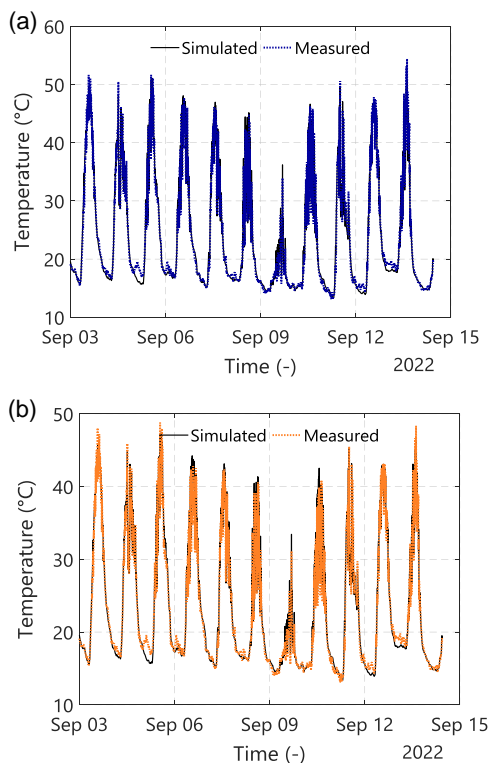


Figure 19. Predicted and measured mini module temperature for a) the standard layout and b) the color layout.

Table 8. Values of MAE, MBE, and RMSE between measured and predicted operating temperature for a standard mini module and a colored mini module.

| | Standard [°C] | Orange [°C] |
|------|---------------|-------------|
| MAE | 0.82 | 0.77 |
| MBE | 0.22 | 0.36 |
| RMSE | 1.15 | 1.15 |

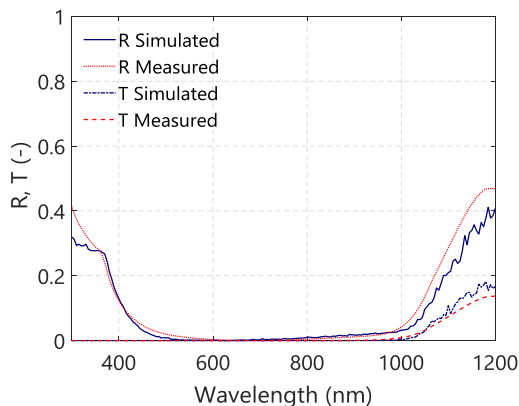


Figure 20. Photograph of the selected solar cell for this work: a 5 in wide SunPower IBC solar cell. On the right, the result from the optical fit based on measurements carried out using the Perkin Elmer Lambda 950 spectrophotometer.

the root-mean-square error (RMSE). The results of these calculations are summarized in **Table 6**.

Results indicated a particularly good agreement for the case of the flat CF (RMSE = 2.36%), and a good agreement for the CF deposited on the random textured glass (RMSE = 5.65%).

The optical model was also validated for angles of incidence above 0° for the case of the textured surface. The measurements of the purple module (based on randomly textured glass) were carried out with a Perkin Elmer Lambda 950 spectrophotometer equipped with an ARTA

Table 9. Estimated two-diode parameters for the SunPower IBC solar cell.

| Parameter | | | Value |
|-------------------------|-------|------------------------|--------|
| Light collected current | (JL) | [mA cm ⁻²] | 37.204 |
| Saturation current 1 | (J1) | [pA cm ⁻²] | 0.14 |
| Ideality factor 1 | (m1) | [-] | 1 |
| Saturation current 2 | (J2) | [nA cm ⁻²] | 3.74 |
| Ideality factor 2 | (m2) | [-] | 2 |
| Shunt resistance | (RSH) | [kΩ cm ²] | 18 |
| Series Resistance | (RS) | [Ω cm ²] | 0.6 |

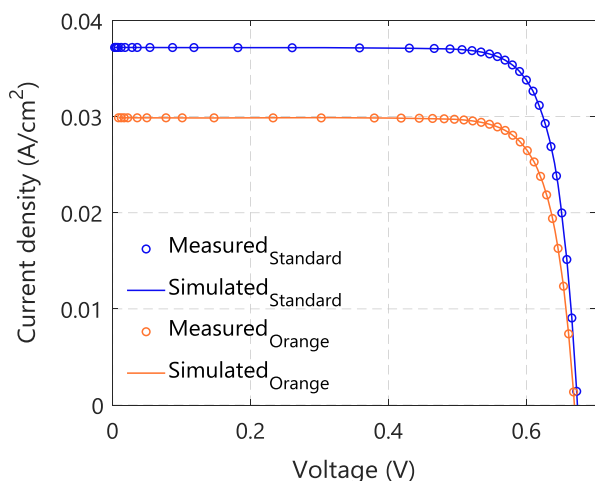


Figure 21. Measured and simulated *J*-*V* curves of an encapsulated IBC solar cell with a standard flat glass and a colored flat glass.

accessory^[38,39] The measurement obtained is known as angular intensity distribution (AID).^[40] It was not possible to validate the optical model by direct comparison of the predicted reflectance, but rather, by comparing the normalized reflection with the AID values obtained experimentally. **Figure 17** presents the results for AoOs of 50° and 70°.

Table 7 presents the calculated accuracy metrics. The value of the RMSE error is significant at AoOs of 70° and above. A probable explanation for this deviation is that GenPro4 considers a uniform layer growth across the textured surface. The growth of the layers on such surfaces does not follow this trend, as explained by Wessels, et al.^[34] and reported by other studies that analyzed this trend on non-flat surfaces.^[41,42] So, for larger optical paths, the deviation between the predicted behavior differed more than for the case of normal incidence.

The orange mini module was taken for temperature measurements under the environmental conditions of Delft, in the Netherlands. The measurements took place from September 3, 2022 through September 14, 2022. T-type thermocouples were attached to the mini modules with aluminum tape and thermal tape for proper insulation. The time resolution of the measurements was 10 s. The mini modules were tilted 30° and oriented toward the south **Figure 18** and **19**.

The predicted temperature from the thermal model was compared to the temperature measurements obtained for the same time resolution. Results show that for both cases, the thermal model predicts with great accuracy the thermal behavior of the mini modules. It is observed also that the color module operates at lower temperatures compared to the standard module. The thermal model, which estimates the spectral behavior of the solar cell and its thermalization losses, predicts very well the impact of the color on the cell operational temperature (see **Table 8**).

For the validation of the electrical model, the optical behavior of the IBC solar cell from SunPower was measured. The resulting fit with the optical model is presented in **Figure 20**.

The electrical behavior of the solar cell was measured (already encapsulated with a 3 mm thick flat glass) on an Class AAA solar simulator. From these measurements, the parameters for the two-diode model were extracted by using the tool provided by PV lighthouse.^[43] The resulting parameters are shown in **Table 9**. The parameters were kept constant, except for the light-collected current, which was scaled down according to the value of *j*_{CF} defined in Equation (2) and estimated by using GenPro4. The resulting *J*-*V* curve was then compared to the measured *J*-*V* of the colored mini module. Results show great agreement, as shown in **Figure 21**. The RSME for the case of the colored mini module was below 1%.

Supporting Information

Supporting Information is available from the Wiley Online Library or from the author.

Conflict of Interest

The authors declare no conflict of interest.

Data Availability Statement

The data that support the findings of this study are available on request from the corresponding author. The data are not publicly available due to privacy or ethical restrictions.

Keywords

colors, design, integration, performance, photovoltaics

Received: April 5, 2023

Revised: June 27, 2023

Published online: July 30, 2023

- [1] W. F. Lamb, T. Wiedmann, J. Pongratz, R. Andrew, M. Crippa, J. G. J. Olivier, D. Wiedenhofer, G. Mattioli, A. A. Khourdajie, J. House, S. Pachauri, M. Figueroa, Y. Saheb, R. Slade, K. Hubacek, L. Sun, S. K. Ribeiro, S. Khennas, S. de la Rue du Can, L. Chapungu, S. J. Davis, I. Bashmakov, H. Dai, S. Dhakal, X. Tan, Y. Geng, B. Gu, J. Minx, *Environ. Res. Lett.* **2021**, *16*, 073005.
- [2] T. Klein, W. R. L. Anderegg, *Sustainable Cities Soc.* **2021**, *73*, 103098.
- [3] R. A. Agathokleous, S. A. Kalogirou, *Energy* **2020**, *191*, 116471.
- [4] T. E. Kuhn, C. Erban, M. Heinrich, J. Eisenlohr, F. Ensslen, D. H. Neuhaus, *Energy Build* **2020**, *231*, 110381.
- [5] C. Ballif, L.-E. Perret-Aebi, S. Lufkin, E. Rey, *Nat. Energy* **2018**, *3*, 438.
- [6] C. R. Reddy, *Performance of Ceramic Ink Printed Colour Photovoltaic Technology*, Delft University of Technology, New York, NY **2018**.
- [7] M. H. Saw, J. P. Singh, Y. Wang, K. E. Birgersson, Y. S. Khoo, *IEEE J. Photovoltaics* **2020**, *10*, 1027.
- [8] T. Masuda, Y. Kudo, D. Banerjee, *Coatings* **2018**, *8*, 282.
- [9] L. M. Yu, J. X. Man, T. Chen, D. Luo, J. Wang, H. Yang, Y. B. Zhao, H. Wang, Y. Yang, Z. H. Lu, *Nano Energy* **2021**, *85*, 105937.
- [10] T. Gewohn, M. R. Vogt, B. Lim, C. Schinke, R. Brendel, *IEEE J. Photovoltaics* **2021**, *11*, 138.
- [11] G. Peharz, K. Berger, B. Kubicek, M. Aichinger, M. Grobbauer, J. Gratzner, W. Nemitz, B. Großschädl, C. Auer, C. Prietl, W. Waldhauser, *Renewable Energy* **2017**, *109*, 542.
- [12] B. Bläsi, T. Kroyer, O. Höhn, M. Wiese, C. Ferrara, U. Eitner, T. E. Kuhn, in *33rd EUPVSEC*, Amsterdam, NL, September 2017, pp. 2–6.
- [13] B. Bläsi, T. Kroyer, T. E. Kuhn, O. Höhn, *IEEE J. Photovoltaics* **2021**, *11*, 1305.
- [14] C. A. Tippets, Y. Fu, A. M. Jackson, E. U. Donev, R. Lopez, *J. Opt.* **2016**, *18*, 065105.
- [15] S. Villa, *Colored PV Modules Based on Interference Filters*, Delft University of Technology, Delft **2018**.
- [16] J. H. Selj, T. T. Mongstad, R. Sondenå, E. S. Marstein, *Sol. Energy Mater. Sol. Cells* **2011**, *95*, 2576.
- [17] L. Zeng, M. Li, Y. Chen, H. Shen, *Sol. Energy* **2014**, *103*, 343.
- [18] M. H. Saw, M. Pravettoni, E. Birgersson, *IEEE J. Photovoltaics* **2022**, *12*, 1533.
- [19] B. Ramkiran, C. K. Sundarabalan, K. Sudhakar, *Case Stud. Therm. Eng.* **2020**, *21*, 100700.
- [20] K. R. McIntosh, M. Amara, F. Mandorlo, M. D. Abbott, B. A. Sudbury, in *AIP Conf. Proceedings*, American Institute of Physics Inc., Maharashtra, IN, August 2018, <https://doi.org/10.1063/1.5049256>.
- [21] M. Amara, F. Mandorlo, R. Couderc, F. Gérenton, M. Lemiti, *EPJ Photovoltaics* **2018**, *9*, 1.
- [22] J. Halme, P. Mäkinen, *Energy Environ. Sci.* **2019**, *12*, 1274.
- [23] M. Pelle, F. Causone, L. Maturi, D. Moser, *Energies* **2023**, *16*, 1991.
- [24] J. C. Ortiz Lizcano, P. Procel, A. Calcabrini, G. Yang, A. Ingenito, R. Santbergen, M. Zeman, O. Isabella, *Prog. Photovoltaics: Res. Appl.* **2021**, *30*, 401.
- [25] R. Santbergen, T. Meguro, T. Suezaki, G. Koizumi, K. Yamamoto, M. Zeman, *IEEE J. Photovoltaics* **2017**, *7*, 919.
- [26] J. Lindon, J. Holmes, G. Tranter, *Encyclopedia of Spectroscopy and Spectrometry*, Academic Press, Elsevier, Oxford, UK **2019**, pp. 337–343.
- [27] H. Kawamura, K. Naka, N. Yonekura, S. Yamanaka, H. Kawamura, H. Ohno, K. Naito, *Sol. Energy Mater. Sol. Cells* **2003**, *75*, 613.
- [28] D. Ristau, H. Ehlers, *Thin Film Optical Coatings*, Springer, New York, NY **2012**, https://doi.org/10.1007/978-3-642-19409-2_6.
- [29] A. Zeileis, K. Hornik, P. Murrell, *Comput. Stat. Data Anal.* **2009**, *53*, 3259.
- [30] G. Sharma, W. Wu, E. N. Dalal, *Color Res. Appl.* **2005**, *30*, 21.
- [31] T. Rose, A. Wollert, *Environ. Impact Assess. Rev.* **2015**, *52*, 24.
- [32] N. Jolissaint, R. Hanbali, J. C. Hadorn, A. Schüler, *Energy Procedia*, Elsevier, Ltd., Lausanne, CH **2017**, pp. 175–180, <https://doi.org/10.1016/j.egypro.2017.07.340>.
- [33] T. C. Loef, *Periodic-Random Modulated Surface Textures*, Delft University of Technology, Delft **2018**.
- [34] A. Wessels, A. Callies, B. Bläsi, T. Kroyer, O. Höhn, *Opt. Express* **2022**, *30*, 14586.
- [35] D. D. Smith, et al., in *2013 IEEE 39th Photovoltaic Specialists Conference (PVSC)*, IEEE, Tampa Bay, US **2013**, pp. 0908–0913.
- [36] Saint-Gobain Glass - Business Unit Photovoltaics, *SGG ALBARINO High Energy Transmittance Extra-White Patterned Glass for the Photovoltaic and Solar Thermal Industry Saint-Gobain Glass Vision, France* **2017**, <https://glassolutions.sk/sites/glassolutions.eu/files/2017-08/ssg-albarino-prospekt.pdf> (accessed: June 2023).
- [37] R. N. Abeyta, *Dissertations and Thesis, Embry-Riddle Aeronautical University, Daytona* **2011**.
- [38] P. A. Van Nijnatten, *Thin Solid Films* **2003**, *442*, 74.
- [39] K. Jäger, O. Isabella, L. Zhao, M. Zeman, *Phys. Status Solidi C* **2010**, *7*, 945.
- [40] K. Jäger, O. Isabella, R. A. C. M. M. Van Swaaij, M. Zeman, *Meas. Sci. Technol.* **2011**, *22*, 105601.
- [41] K. Pfeiffer, U. Schulz, A. Tünnermann, A. Szeghalmi, *Coatings* **2017**, *7*, 118.
- [42] A. Ingenito, S. Luxembourg, P. Spinelli, A. Weeber, O. Isabella, M. Zeman, in *2015 IEEE 42nd Photovoltaic Specialist Conf., PVSC 2015*, Institute of Electrical and Electronics Engineers Inc., Piscataway, NJ, December 2015, <https://doi.org/10.1109/PVSC.2015.7356157>.
- [43] P. Lighthouse, <https://www.pvlighthouse.com.au> (accessed: October 2022).
- [44] G. Yang, R. van Swaaij, O. Isabella, Patent Cooperation Treaty (PCT), WO2015093966A1 **2015**.
- [45] M. R. Vogt, H. Hahn, H. Holst, M. Winter, C. Schinke, M. Köntges, R. Brendel, P. P. Altermatt, *IEEE J. Photovoltaics* **2016**, *6*, 111.
- [46] M. R. Vogt, H. Holst, H. Schulte-Huxel, S. Blankemeyer, R. Witteck, D. Hinken, M. Winter, B. Min, C. Schinke, I. Ahrens, M. Köntges, *Energy Procedia* **2016**, *92*, 523.